Structural Insights into the Interaction of the Nip7 PUA Domain with Polyuridine RNA[†,‡]

Patrícia P. Coltri,[§,#] Beatriz G. Guimarães,[§,#] Daniela C. Granato,[||] Juliana S. Luz,[||] Elaine C. Teixeira,[§] Carla C. Oliveira,[||] and Nilson I. T. Zanchin*[,§]

Center for Structural Molecular Biology, Brazilian Synchrotron Light Laboratory, LNLS, Rua Giuseppe Maximo Scolfaro 10000, P.O. Box 6192, CEP13083-970, Campinas SP, Brazil, and Department of Biochemistry, Institute of Chemistry, University of São Paulo, Av. Prof. Lineu Prestes, 748, São Paulo, SP, 05508-900, Brazil

Received August 7, 2007; Revised Manuscript Received October 4, 2007

ABSTRACT: The conserved protein Nip7 is involved in ribosome biogenesis, being required for proper 27S pre-rRNA processing and 60S ribosome subunit assembly in *Saccharomyces cerevisiae*. Yeast Nip7p interacts with nucleolar proteins and with the exosome subunit Rrp43p, but its molecular function remains to be determined. Solution of the *Pyrococcus abyssi* Nip7 (PaNip7) crystal structure revealed a monomeric protein composed by two alpha-beta domains. The N-terminal domain is formed by a five-stranded antiparallel β-sheet surrounded by three α-helices and a 3_{10} helix while the C-terminal, a mixed β-sheet domain composed by strands β8 to β12, one α-helix, and a 3_{10} helix, corresponds to the conserved PUA domain (after *P*seudo-*U*ridine synthases and *A*rchaeosine-specific transglycosylases). By combining structural analyses and RNA interaction assays, we assessed the ability of both yeast and archaeal Nip7 orthologues to interact with RNA. Structural alignment of the PaNip7 PUA domain with the RNA-interacting surface of the ArcTGT (archaeosine tRNA-guanine transglycosylase) PUA domain indicated that in the archaeal PUA domain positively charged residues (R151, R152, K155, and K158) are involved in RNA interaction. However, equivalent positions are occupied by mostly hydrophobic residues (A/G160, I161, F164, and A167) in eukaryotic Nip7 orthologues. Both proteins can bind specifically to polyuridine, and RNA interaction requires specific residues of the PUA domain as determined by site-directed mutagenesis. This work provides experimental verification that the PUA domain mediates Nip7 interaction with RNA and reveals that the preference for interaction with polyuridine sequences is conserved in *Archaea* and eukaryotic Nip7 proteins.

Eukaryotic ribosome biogenesis takes place mainly in the nucleolus where a large pre-rRNA, containing the sequences of the mature 18S, 5.8S, and 25S/28S rRNAs separated by external and internal spacer sequences, is transcribed by RNA polymerase I, and the 5S rRNA is transcribed by RNA polymerase III. The pre-rRNA is assembled with processing factors concomitantly with transcription, undergoing subsequently extensive endo- and exonucleolytic cleavage and covalent modification to generate the mature rRNAs (*1*, *2*). Major pre-rRNA processing and ribosome assembly steps have already been described and a large number of factors identified especially in the yeast model system. The large *Saccharomyces cerevisiae* 35S pre-rRNA is assembled into a 90S particle, which is rapidly converted into the pre-40S and the pre-60S preribosomal particles. While the pre-40S particles are further processed in the cytoplasm, pre-60S pre-rRNAs undergo several endo- and exonucleolytic digestions before export to the cytoplasm, where ribosome assembly terminates (*1*, *3*). Important progress has recently been made regarding the identification of the components of the preribosomal complexes. The 90S preribosome contains the 35S pre-rRNA, the U3 snoRNP, 40S subunit processing factors and a large number of 40S subunit ribosomal proteins, along with a small number of 60S ribosomal proteins (*3*). Characterization of the U3 snoRNP led to the identification of the small subunit processing complex, termed SSU processome, which contains 28 proteins required for maturation of the 18S rRNA and 40S subunit biosynthesis (*4*). Absence of 27S pre-rRNA processing factors in the 90S preribosome indicates that the 60S subunit biogenesis factors and structural proteins join the complex later in the process (*4*−*6*).

Nip7p[1] is a conserved protein component of yeast pre-60S complexes (*5*) that is essential for cell viability and for biosynthesis of 60S ribosome subunits. It was initially identified in yeast as required for processing of the 27S pre-rRNA to form the mature 25S and 5.8S rRNAs (*7*). Accumulation of unprocessed 27S pre-rRNA in Nip7p-depleted cells implicates Nip7p in the processing of the internal transcribed spacer 2 (ITS2) (*7*). It localizes to the

[†] This work was supported by FAPESP grants CEPID/CBME-98/14138-2, SMolBNet-00/10266-8, and 06/02083-7 to N.Z. and B.G.G., and 03/06031-3 to C.C.O.

[‡] Coordinates and structure factors for the PaNip7 crystal structure were deposited at RCSB Data Bank with accession number 2P38.

* Corresponding author. Tel: 55 19 3512 1113, fax: 55 19 3512 1004, e-mail: zanchin@lnls.br.

[§] Brazilian Synchrotron Light Laboratory.

[||] University of São Paulo.

[#] These authors contributed equally to this work.

10.1021/bi7015876 CCC: $37.00
Published on Web 11/15/2007

Table 1: Plasmids Used in This Study

plasmid	relevant features	reference
pCYTEX-PaNip7	*P. abyssi* Nip7, Amp^R	(*21*)
pET-PaNip7$^{R151A/R152A}$	*P. abyssi* His-PaNip7-R151A/R152A, Kan^R	this study
pET-PaNip7$^{K155A/K158A}$	*P. abyssi* His-PaNip7-K155A/K158A, Kan^R	this study
pET28-Nip7	*S. cerevisiae* His-Nip7, Kan^R	this study
pET-Nip7$^{I161A/F164A}$	*S. cerevisiae* His-Nip7-I161A/F164A, Kan^R	this study
pGEM-5.8S	*S. cerevisiae* 5.8S rRNA, Amp^R	(*10*)
pGEM-5ETS	*S. cerevisiae* 5-ETS, Amp^R	this study
pGEM-ITS2	*S. cerevisiae* ITS2, Amp^R	this study

nucleolus but was also found to sediment in the region of free 60S subunits in sucrose density gradients (*7*) which is consistent with its presence in pre-60S complexes (*5*). Neither Nip7p nor its nucleolar interacting partners, Nop8p and Nop53p, whose molecular function also remains to be described, seem to possess intrinsic catalytic activity (*8*−*10*). Yeast Nip7p interacts also with the exosome subunit Rrp43p (*9*). Although an intact exosome is required for maturation of the 3′-end of the 5.8S rRNA following cleavage of the 27S pre-rRNA in ITS2 (*11*, *12*), our analyses of Nip7p-deficient yeast strains failed to provide a functional link connecting Nip7p to the exosome function. The interaction between the yeast proteins Nip7p-Nop8p is conserved by their human orthologues (*13*), and recently we have shown that the human Nip7 can be pulled-down from HEK293 cell extracts by the GST-tagged Shwachman−Bodian−Diamond syndrome associated protein (*14*), indicating that both proteins are part of the same complex, a finding that implicates Nip7p in 60S ribosome biogenesis also in humans.

Nip7 orthologues share a highly similar two-domain architecture with the C-terminal region corresponding to the conserved PUA domain. This domain, named after pseudouridine synthases and archaeosine-specific transglycosylases (*15*), was initially described in tRNA modifying enzymes and in pseudo-uridine synthases from *Archaea* and eukaryotes (*16*−*18*) and has been proposed to mediate protein−RNA interactions. However, the PUA domain was also found in the human candidate oncogene MCT1, which was reported to interact with the mRNA cap translation factor complex via its PUA domain and to modulate translation of a subset of mRNAs (*19*). Interestingly, one of the domains of the *Escherichia coli* glutamate 5-kinase, an enzyme with function not related to RNA metabolism, also contains a PUA domain (*20*).

Despite the information obtained from yeast conditional mutant strains and from protein interaction analyses (*7*, *10*), the molecular function of Nip7p remains elusive, and the scope of this work was to investigate the role played by Nip7 and particularly by its conserved C-terminal PUA domain in regard to RNA interaction. Following solution of the crystal structure of the archaeal Nip7 orthologue from *Pyrococcus abyssi* (PaNip7), comparative structural analyses revealed that the residues involved in RNA contacts are conserved in archaeal PUA domains, but equivalent residues are replaced by mostly hydrophobic residues in the PUA domain of eukaryotic Nip7. The initial working hypothesis involved the possible interaction of Nip7p with pre-rRNA sequences. Since yeast Nip7p showed low binding affinity for several regions of the pre-rRNA, additional RNA binding studies were conducted which revealed that both the yeast Nip7p and PaNip7 orthologues can bind directly to polyuridine sequences, indicating conserved functional features among the orthologues. The results presented in this work also include mutational analyses of the PUA domain residues predicted to mediate yeast Nip7p and PaNip7 interaction with RNA and have established a role for the PUA domain of Nip7 proteins in binding of uridine-rich RNAs.

EXPERIMENTAL PROCEDURES

Plasmids and Bacterial Strains. Plasmids used in this study are listed in Table 1, and cloning procedures are summarized below. Plasmid pET28-Nip7p for expression of histidine-tagged yeast Nip7p was generated by transferring the 546 bp Nip7p coding sequence from pCYTEX-Nip7 (*7*) to pET28a using the NdeI/BamHI restriction sites. Plasmid pCYTEX-PaNip7 has been described previously (*21*). The PaNip7 PaNip7$^{R151A/R152A}$ and PaNip7$^{K155A/K158A}$ mutant variants were constructed by PCR amplification of the PaNip7 coding sequence using plasmid pCYTEX-PaNip7 as DNA template, oligonucleotide ONZ184 as forward primer (5′AGG AAG CAT ATG AGT GGT GAG CTG AGG 3′) and either oligonucleotide ONZ519 (5′ GGA TCC CTA ACG CCT TAA AAA CTC CCC AAC ATC CTT TAA ATT TTT TAT AAA TGC TGC ATC GCT CTT CGG 3′) or ONZ520 (5′GGA TCC CTA ACG CCT TAA AAA CTC CCC AAC ATC CGC TAA ATT TGC TAT AAA TCT TCT ATC GC 3′) as reverse primers, containing the base substitutions to replace either R151 and R152 or K155 and K158 by alanine residues. The resulting PCR products were subsequently inserted into the pETTEV plasmid (*22*) using the NdeI/BamHI restriction sites, generating plasmids pET-PaNip7$^{R151A/R152A}$ and pET-PaNip7$^{K155A/K158A}$. These plasmids express histidine-tagged proteins to allow purification by metal chelating affinity chromatography. Construction of the yeast Nip7p$^{I161A/F164A}$ mutant was performed by two sequential PCR steps. Initially, an 80 bp fragment of the Nip7p C-terminal region was PCR-amplified using oligonucleotide ONZ522 as forward primer (5′ GGT GCA GTT GCT GCC AGA CAA GCA GAT ATT GG 3′), containing base substitutions to replace I161 and F164 by alanine, and oligonucleotide ONZ283 as reverse primer (5′ GCA GGT CGA CCT AAG TAA ACA AGG TGT C 3′). The resulting PCR product was used as reverse primer in combination with

[1] Abbreviations: Nip7p, *Saccharomyces cerevisiae* nuclear import protein 7; PaNip7, *Pyrococcus abyssi* Nip7p orthologue; HsNip7, *Homo sapiens* Nip7p orthologue; PUA domain, *P*seudo-*U*ridine synthases and *A*rchaeosine-specific transglycosylases-containing domain; ArcTGT, *P. horikoshii* archaeosine tRNA-guanine transglycosylase; Rrp43p, *S. cerevisiae* ribosomal RNA processing protein 43; Nop8p, *S. cerevisiae* nucleolar protein 8; Nop53p, *S. cerevisiae* nucleolar protein 53; EMSA, electrophoretic mobility shift assay; ITS1, internal transcribed spacer sequence 1; ITS2, internal transcribed spacer sequence 2; 5′ ETS, 5′ external transcribed spacer sequence; RNase A, ribonuclease A.

oligonucleotide ONZ521 (5′ CGG CAT ATG AGA CAG CTA ACA GAA GAA GAG 3′) for PCR-amplification of the complete Nip7p coding sequence containing the I161A/F164A mutations, which was subsequently subcloned into the pETTEV plasmid (*22*) using the NdeI/SalI restriction sites, generating plasmid pET-Nip7$^{I161A/F164A}$. The pre-rRNA coding sequence from the 5′-ETS up to cleavage site A_0 and the ITS2 sequence were PCR-amplified using *S. cerevisiae* genomic DNA and cloned into the plasmid pGEM-T (Promega), generating pGEM-5′ETS and pGEM-ITS2. Construction of plasmid pGEM-5.8S has been described previously (*10*).

All plasmid constructs were verified by DNA sequencing analysis. *E. coli* strains DH5α and BL21(DE3), used for DNA amplification and protein expression, respectively, were manipulated according to standard techniques (*23*).

Recombinant Proteins Expression and Purification. Expression and purification of PaNip7 has been described previously (*21*). Expression of proteins from pET28a-derivative plasmids was performed in *E. coli* BL21(DE3) cells incubated in LB medium containing kanamycin (50 μg mL^{-1}) at 30 °C. At an OD_{600} of ~0.8, the cultures were induced by adding 0.5 mM IPTG and incubating at 30 °C for further 4−6 h. Cells were harvested by centrifugation, suspended in buffer containing 50 mM sodium phosphate pH 7.2, 100 mM NaCl, 10% glycerol, and 0.5 mM phenylmethylsulfonyl fluoride (PMSF), and treated with lysozyme (50 μg mL^{-1}) for 30 min on ice. Subsequently, cells were disrupted by sonication, and the his-tagged proteins were initially purified by metal-chelating affinity chromatography on Ni-NTA columns (Qiagen), using 20−200 mM imidazole gradients for elution. Nip7p was further purified by chromatography on a heparin-sepharose column (GE Healthcare) using the same buffer as above for binding and a 50 mM to 1 M KCl gradient for elution. PaNip7$^{R151A/R152A}$ and PaNip7$^{K155A/K158A}$ were purified further by ion exchange chromatography on a mono-Q column (GE Healthcare) using buffer containing 10 mM Tris-HCl pH 7.0, 1 mM EDTA, 50 mM NaCl, and 5 mM β-mercaptoethanol for binding and a 50 mM to 1 M NaCl gradient for elution. The Nip7p$^{I161A/F164A}$ protein was refolded from inclusion bodies as described previously for the wild-type Nip7p (*7*). Following refolding, Nip7p$^{I161A/F164A}$ was purified by metal-chelating affinity chromatography on a Ni-NTA column (Qiagen) using the procedure described above.

UV Cross-Linking Assays. For analysis of the interaction of yeast Nip7p with sequences of the yeast pre-rRNA, the RNA fragments corresponding to the 5.8S rRNA, the 5′ spacer (5′-ETS), the ITS2 spacer sequences, and an unrelated control RNA were transcribed *in vitro* with T7 or SP6 RNA polymerases using linearized plasmids in the presence of 10 μCi of [α-^{32}P]-UTP (*10*). *In vitro* transcription of linearized plasmids pGEM-5′ETS, pGEM-ITS2, and pGEM-5.8S using T7 RNA polymerase generate RNAs of 550, 220, and 180 nucleotides, respectively. The unrelated RNA was transcribed *in vitro* from linearized pBlueScript, generating a 65-nucleotide RNA. One picomole of radiolabeled RNA was incubated with different amounts of purified His-Nip7p in buffer A containing 20 mM Tris-Cl pH 8.0, 5 mM magnesium acetate, 150 mM potassium acetate, 0.2% v/v Triton X-100, 1 mM DTT, and 1 mM PMSF with 0.8 U RNAse OUT (Invitrogen) for 30 min at 37 °C. A 5−20 pmol amount of cold RNAs generated by parallel *in vitro* transcription of the plasmids cited above were used in the competition assays. UV cross-linking was performed by placing RNA−protein complexes on ice and irradiating for 5 min at 260 nm using a Fotodyne transilluminator (Stratagene). Subsequently, samples were treated with 10 μg of RNase A for 30 min at 37 °C. Complexes were resolved on 6% denaturing polyacrylamide gels using 20 mM CAPS pH 11.0 (*N*-cyclohexyl-3-aminopropanesulfonic acid) as buffer and visualized on a Phosphorimager. Relative band intensities were quantified by volume integration using the Image Quant software v. 5.0 (Molecular Dynamics).

Electrophoretic Mobility Shift Assays (EMSA). For EMSA under native conditions, 20 pmol of the RNA oligoribonucleotides poly-$G_{(18)}$, poly-$A_{(25)}$, poly-$U_{(25)}$, and poly-$C_{(25)}$ were [^{32}P]-labeled using 1 U T4 PNK (Fermentas) and 20 μCi [γ^{32}P]-ATP. A 0.4 pmol amount of each [^{32}P]-labeled oligoribonucleotide was incubated with different amounts of the indicated proteins in buffer A for 30 min at 37 °C. Complexes were resolved on 8% polyacrylamide gels using TBE buffer pH 8.0 for electrophoresis and visualized on a Phosphorimager. Relative band intensities were quantified by volume integration using the Image Quant software v. 5.0 (Molecular Dynamics).

Crystallization and Data Collection of the Pyrococcus abyssi Nip7p Orthologue. PaNip7 was crystallized as described previously using the vapor diffusion method (*21*). The best crystals were obtained using 100 mM HEPES buffer pH 7.2 and 4.1 M NaCl as precipitant. Data collection was performed at 100 K at the D03B-MX1 beam line of the Brazilian Synchrotron Light Laboratory using 1.427 Å radiation and recorded on a marCCD165 detector. Data from native crystals were processed to 1.8 Å resolution. Iodide derivative crystals were obtained by the quick cryosoaking technique (*24*, *25*) and diffracted to 1.9 Å resolution (*21*). Statistics from native and derivative data collection have been described previously by Coltri and co-workers (*21*).

Structure Solution and Refinement. The structure of PaNip7 was solved using the SIRAS method. At the time PaNip7 crystals were obtained, no structure from homologous proteins was available in the PDB. Seven I^- sites with occupancies greater than 0.7 were found with the program SHELXD (*26*) using only anomalous data from the derivative crystal. According to the Matthews coefficient calculation, the asymmetric unit should contain 332 residues (two monomers); therefore, SHELXD results indicated the presence of at least one anomalous scatterer per approximately 47 residues. Refinement of heavy atoms parameters and calculation of phases were carried out with SHARP (*27*) using data from native and derivative crystals. An improved electron density map (Supporting Information Figure 1) was obtained by solvent flattening with SOLOMON (*28*). The starting model was built using the program ARP/wARP (*29*). Fifty cycles of autobuilding resulted in seven polypeptide chain fragments containing a total of 289 residues (out of 332). The model was manually completed using the program O (*30*), and structure refinement was carried out with REFMAC (*31*) from the CCP4 package (*32*). Refinement cycles were alternated with visual inspection of the electron density maps and model rebuilding with the program O (*30*). During the final cycles, water molecules were added using the program ARP/wARP (*29*). The final model has an R_{factor}

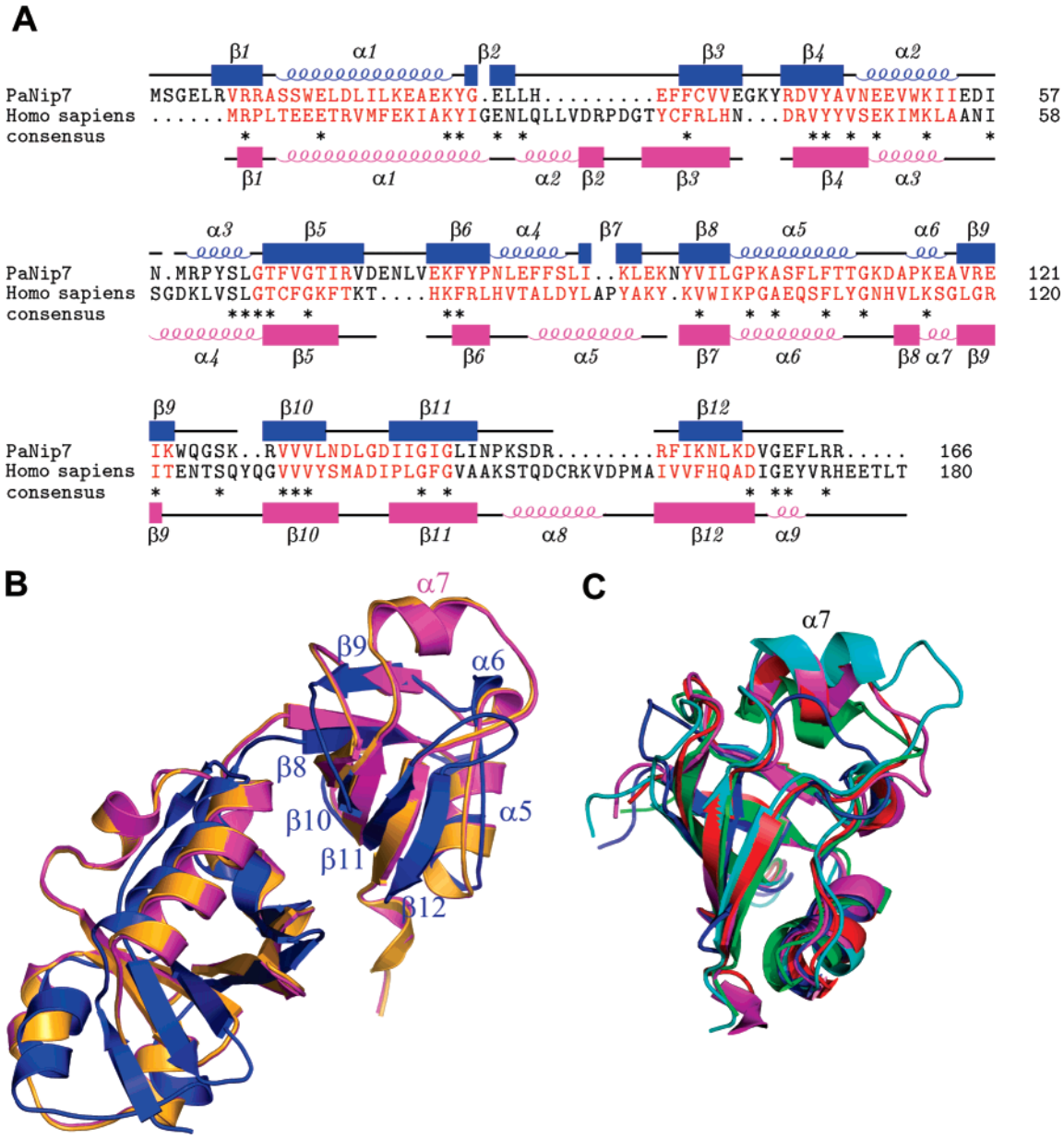

FIGURE 1: Structural comparison of Nip7 proteins. (A) Structure-based sequence alignment of human and *P. abyssi* Nip7 showing the insertion/deletion regions. Secondary structures are assigned on the top (PaNip7) and on the bottom (human Nip7). Structurally aligned residues are represented in red. (B) Superposition of PaNip7 (blue) and human Nip7 (magenta) crystallographic structures and *S. cerevisiae* Nip7p homology model (orange). Secondary structure elements of PaNip7 PUA domain and helix α7 in human and yeast Nip7 are indicated. (C) Superposition of PUA domains showing overall structural conservation and local differences: PaNip7 (blue), human Nip7 (PDB code 1SQW, magenta), *P. horikoshii* tRNA-guanine transglycosylase (PDB code 1J2B,green), *T. maritima* tRNA pseudouridine synthase (PDB code 1ZE1,cyan), *P. abyssi* Cbf5 (PDB code 2AUS,red). The region corresponding to helix α7, not found in PaNip7, is indicated.

of 20.7% (R_{free} = 25.7%) to 1.8 Å resolution with good overall stereochemistry. As defined by the program PROCHECK (*33*) all non-glycine and non-proline residues fall in the most favored or additionally allowed regions of the Ramachandran plot. Further details of refinement are presented in Table 2.

Molecular Modeling of Saccharomyces cerevisae Nip7p. The Nip7p homology model was generated using the SWISS-MODEL homology-modeling server (*34*). Atomic coordinates of human Nip7 homologue (PDB code 1SQW) were used as template. Pairwise alignment resulted in sequence identity of 56.8% between template and target with no gaps. High sequence identity allowed modeling of a continuous chain containing residues 1 to 176. After structure refinement by energy minimization, the final model presented good overall stereochemistry.

RESULTS

Crystal structure of Pyrococcus abyssi Nip7 and Comparison with Eukaryotic Orthologues. Structural analyses were performed in order to obtain information on the mechanism of Nip7p PUA domain interaction with RNA. The crystal structure of the human Nip7p orthologue (HsNip7) has already been described (*35*; PDB code 1SQW), showing a two-domain architecture in which the C-terminal domain corresponds to the conserved PUA domain. In this work, we describe the crystal structure of the *Pyrococcus abyssi* Nip7 orthologue, PaNip7, which was solved by single isomorphous replacement methods with anomalous scattering (SIRAS) using diffraction data from a native crystal and from an iodide derivative (*21*). The model was refined at 1.8 Å

Table 2: Refinement Statistics

resolution range (Å)	51.99−1.80
no. of reflections	31334
protein atoms	2443
water molecules	252
R_{factor}/R_{free} (%)	20.7/25.7
rms deviation from ideality	
bonds (Å)	0.016
angles (deg)	1.710
mean B-values (whole chain) (Å^2)	
monomer A	28.7
monomer B	28.8
solvent atoms	39.2
Ramachandran plot (%)	
most favored regions	92.0
additional allowed regions	8.0

resolution to a final R_{factor} of 20.7% (R_{free} = 25.7%). The final atomic model of PaNip7 includes two crystallographically independent monomers and 252 water molecules. The quality of the electron density allowed modeling of residues 5 to 159 (out of 166) in both monomers. A superposition of the symmetrically independent monomers shows no structural differences and results in an overall rms deviation of 0.11 Å for the 154 common Cα atoms. The two independent monomers associate in a head-to-tail orientation generating a dimer. The interface between the monomers buries a total of ~700 Å^2 of solvent-accessible area per molecule, or ~8% of its total surface. These values led us to suppose that the dimer formation was induced by crystallization and has no biological relevance. In fact, results of gel filtration experiments and dynamic light scattering support this hypothesis (data not shown). The PaNip7 monomer is composed of two alpha-beta domains (Figure 1). The larger N-terminal domain contains a five-stranded antiparallel β-sheet surrounded by three α-helices and one 3_{10} helix (α3). The C-terminal domain that corresponds to the putative RNA-binding domain (PUA) comprises residues 95 to 159 and contains a mixed β-sheet composed of strands β8 to β12, one α-helix, and one short 3_{10} helix (α6) (Figure 1).

A comparison of the PaNip7 atomic coordinates with the contents of the Protein Data Bank using the SSM service (*36*) identified structural alignment with HsNip7, the human Nip7p orthologue (PDB code 1SQW) (22% amino acid identity) and with a conserved hypothetical protein from *Thermoplasma acidophilum* (15% amino acid identity) (not published, PDB code 1Q7H). Superposition of the PaNip7 structure with the orthologues from *H. sapiens* and *T. acidophilum* resulted in overall rms deviations of 2.13 Å (114 Cα aligned) and 1.92 Å (102 Cα aligned), respectively. Despite the overall structural similarity HsNip7 and PaNip7 differ in the C-terminal PUA domain, where HsNip7 presents a large insertion between β-sheets β11 and β12 including residues 149 to 156, which form helix α7, not present in the PaNip7 structure (Figure 1). Yeast and human Nip7 orthologues share an overall 56.8% amino acid identity and 75% similarity. Since there is no crystal structure available for Nip7p, we took advantage of this high similarity and constructed a homology model of Nip7p to help us interpret the RNA interaction data. As expected, the *S. cerevisiae* Nip7p homology model and the HsNip7 crystallographic structure show a perfect superposition, with overall rms deviation of 0.09 Å (all Cα aligned) (Figure 1B).

Nip7p PUA Domain Structure Analysis and RNA-Interacting Residues. Despite the low sequence similarity among proteins from eukaryotes and *Archaea*, the PUA domain presents a conserved three-dimensional structure (Figure 1C). Superposition of PaNip7 and HsNip7 PUA domain structures resulted in overall rms deviations of 0.90 Å for 58 Cα aligned. Comparison with other PUA domains also resulted in a good structural superposition (*P. horikoshii* tRNA-guanine transglycosylase, PDB code 1J2B: rmsd = 1.15 Å for 58 Cα aligned; *T. maritima* tRNA pseudouridine synthase, PDB code 1ZE1: rmsd = 1.40 Å for 61 Cα aligned; *P. abyssi* Cbf5, PDB code 2AUS: rmsd = 1.08 Å for 58 Cα aligned). Interestingly, helix α7, the main structural difference between PaNip7 and HsNip7p PUA domains, is also found in PUA domains from other archaeal proteins (Figure 1C).

The crystal structure of *P. horikoshii* tRNA-guanine transglycosylase (ArcTGT) in complex with tRNA revealed the residues from domain C3 (the PUA domain) involved in RNA interaction (*37*; PDB code 1J2B). Structural comparison of PUA domains shows that most of the ArcTGT residues which participate in RNA interaction are structurally conserved in PaNip7 (Figure 2, Table 3). In the PaNip7 structure, arginine and lysine residues (R151, R152, K155, K158) form a positively charged path which may be

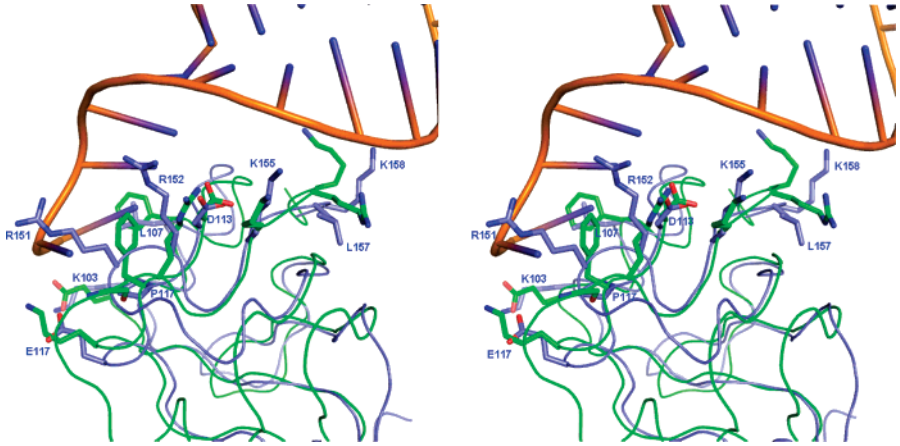

FIGURE 2: Residues of PUA domain involved in RNA interaction. Stereoview of a structural comparison of PUA domains of PaNip7 (blue) and archaeosine tRNA-guanine transglycosylase in complex with tRNA (ArcTGT, green). The ArcTGT residues involved in tRNA interactions and the structurally correspondent side-chains in PaNip7 structure are shown in sticks. The labels refer to PaNip7 residues and the RNA molecule is represented in orange-blue.

Table 3: Residues of Archaeosine tRNA-Guanine Transglycosylase (ArcTGT) PUA Domain Involved in RNA Interactions and Structurally Equivalent Residues in Nip7p Proteins from *P. abyssi*, *S. cerevisiae*, and *H. sapiens*

protein	residue									
ArcTGT	E515	F519	D525	F527	K529	G572	R573	K576	R578	K579
PaNip7	K103	L107	D113	P117	E117	R151	R152	K155	L157	K158
ScNip7	N102	P106	H112	L114	A116	G160	I161	F164	Q166	A167
HsNip7	G102	S106	H112	L114	S116	A160	I161	F164	Q166	A167

implicated in RNA binding, in a similar manner as described for the tRNA-ArcTGT complex (Figure 2, Table 3). Interestingly, analysis of the HsNip7 crystallographic structure and the Nip7p homology model revealed a charge pattern different from PaNip7 (Figure 3). In particular, PaNip7 arginine and lysine residues putatively involved in RNA interaction are not structurally conserved in the yeast and human counterparts, the same region being occupied by a glycine and three residues with hydrophobic side chain (Table 3). As shown in Figure 3B, the PUA domain of PaNip7 displays a highly positive electrostatic surface in the predicted RNA-interacting region, whereas the PUA domain of Nip7p displays an overall hydrophobic surface with a positively charged patch restricted to the region containing residues K100, K115, and R154 that are not conserved in PaNip7. This finding indicates that in these proteins, the PUA domain−RNA contacts might be mediated by different interactions.

Nip7p Interacts Directly with Polyuridine. Given the requirement of Nip7p for 27S pre-rRNA processing in yeast, Nip7p was expected to interact with regions of the pre-rRNA or with sequences corresponding to the mature rRNAs. In order to test this hypothesis, a series of *in vitro* RNA interaction assays were initially performed by using recombinant histidine-tagged Nip7p and *in vitro* transcribed RNAs corresponding to the 5.8S rRNA, ITS2 and 5′-ETS regions of the yeast pre-rRNA. An unrelated RNA transcribed from vector pBluescript (pBS) was used as a nonspecific competitor. Nip7p did not produce shifted bands on electrophoretic mobility shift assays with these RNAs under native conditions (data not shown), indicating that the affinity of Nip7p for the pre-rRNAs sequences tested is low. However, Nip7p interaction with RNAs derived from the 35S yeast pre-rRNA can be observed in RNase protection assays, in which RNA-Nip7p complexes were UV-cross-linked and treated with RNase A prior to denaturing polyacrylamide gel electrophoresis (Figure 4). In an attempt to determine whether Nip7p shows a higher affinity for a particular pre-rRNA region, we performed competition experiments. In these assays, 20 pmol Nip7p bound to 1 pmol of [^{32}P]-labeled RNA were incubated with unlabeled RNAs at concentrations of 5, 10, and 20 pmol (Figure 4). Although ITS2 was a somewhat more efficient competitor relative to the other RNAs, particularly relative to the unrelated RNA derived from the pBluescript plasmid (Figure 4), this experiment does not indicate that Nip7p recognizes a specific sequence of the RNAs tested.

In order to determine whether Nip7p shows a higher affinity to a particular RNA sequence, we performed a second round of experiments using homo-oligoribonucleotides in native electrophoretic mobility shift assays. Interestingly, these assays revealed that Nip7p binds specifically to poly-U (Figure 5A). Parallel assays were performed also with PaNip7, which also showed specific binding to poly-U. No

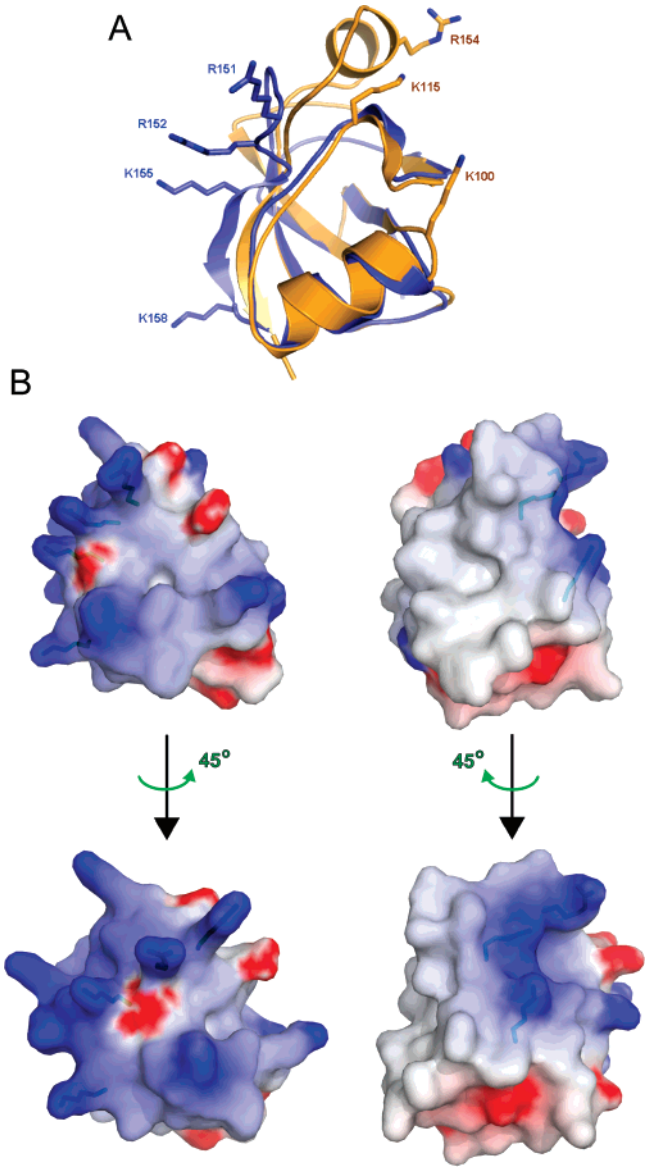

FIGURE 3: Structural comparison of the *P. abyssi* and *S. cerevisiae* Nip7 PUA domains. (A) Overlay of the PaNip7 (blue) and Nip7p (orange) PUA domains. Positively charged residues which could form a basic pathway for RNA interaction are showed in sticks and labeled. (B) Electrostatic surfaces of the PaNip7 (left) and Nip7p (right) PUA domains colored by charge, from red (negative) to blue (positive). The upper panel shows the electrostatic surface in the same position as shown in A. The lower panel shows the domains rotated by 90°, resulting from a 45° rotation to the right for the PaNip7 PUA domain (left) and from a 45° rotation to the left for the Nip7p (right) PUA domain, as indicated by the green arrows, to better view the positively charged regions. Residues indicated in A are represented in sticks.

band corresponding to a mobility shift equivalent to the one observed for poly-U was detected for the poly-C, poly-A, and poly-G probes, although in the case of yeast Nip7p, the signal of the probe disappeared from the free probe region

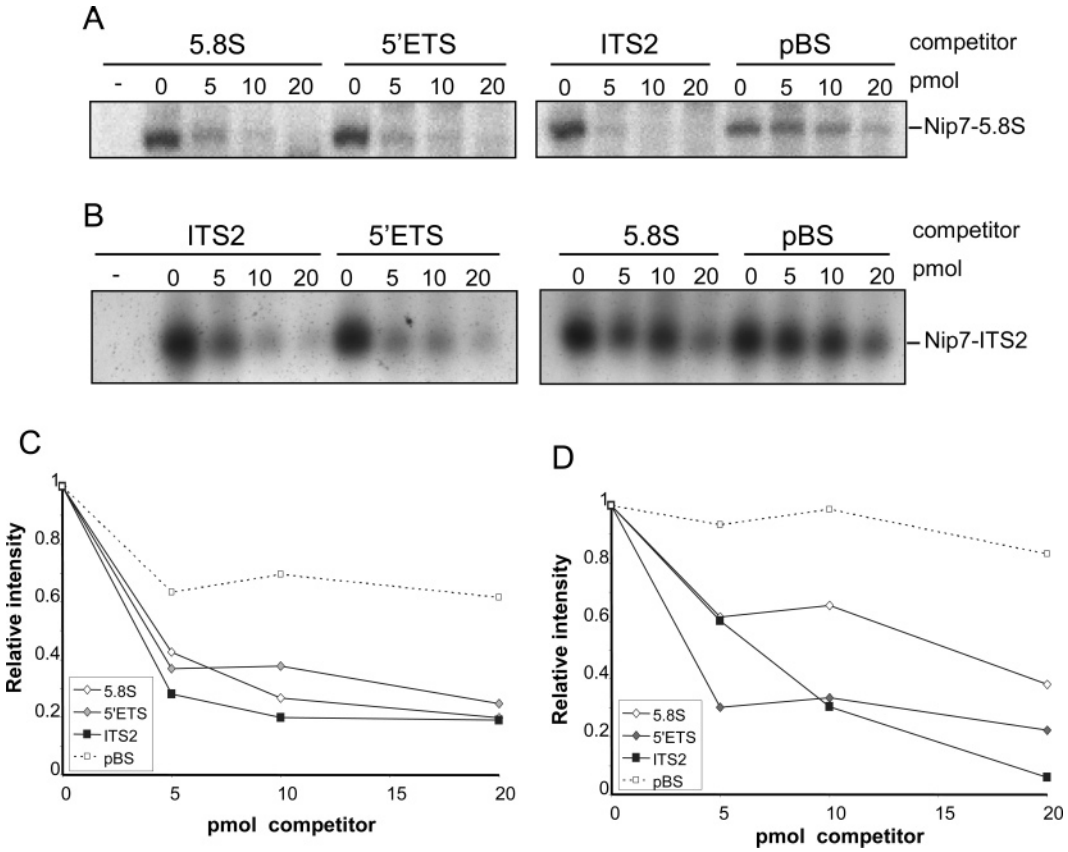

FIGURE 4: Analysis of yeast Nip7p interaction with pre-rRNA sequences. (A and B) 20 pmol of Nip7p was incubated with 1 pmol of *in vitro* transcribed [^{32}P]-labeled 5.8S RNA and [^{32}P]-labeled ITS2 RNA, respectively. Subsequently the reactions were incubated with increasing amounts (0, 5, 10, and 20 pmol) of unlabeled competitor RNAs as indicated. Samples were submitted to UV cross-linking for 5 min, treated with RNase A, and resolved on denaturing polyacrylamide gels using 20 mM CAPS pH 11.0 both as electrophoresis and gel buffer. Protein−RNA complexes were visualized by autoradiography. Lanes marked with "−" indicate the controls without Nip7p. (C and D) Quantitation of the assays shown in A and B, respectively. The graphs show the relative intensity of the bands in the competition reactions as compared to the reaction where no unlabeled competitor was added (lane 0).

and a band appeared in the well region (Figure 5A, arrowhead). We interpreted the presence of the band in the well as resulting from unspecific binding and aggregation. Although poly-G is known to adopt higher order structures that may affect protein interaction, it was included in the assay to have a complete set of RNA homopolymers tested. Binding of Nip7p and PaNip7 to poly-U was concentration-dependent (Figure 5B). Although equivalent amounts of protein and of ^{32}P-labeled poly-U probe were used for both Nip7p and PaNip7, the signal for Nip7p-poly-U complexes was consistently weaker in all assays performed. The signal of the free probe diminishes with the increase of the Nip7p concentration in the binding reaction, and part of the material is retained in the well, suggesting that part of the sample does not enter the gel.

Mutation Analysis of RNA-Interacting Residues of the Nip7 PUA Domain. The fact that both *P. abyssi* and *S. cerevisiae* Nip7 orthologues show preference for binding to poly-U RNAs is quite intriguing (Figure 5). In the case of PaNip7, evidence from structure comparison of its PUA domain with the PUA domain of ArcTGT indicates that RNA interaction is mediated by contacts of positively charged residues (R151, R152, K155, K158) with phosphates of the RNA (Figure 2, Table 3). In order to test whether these residues are involved in RNA interaction, two mutant clones were generated. Both are double mutants, one containing alanine residues at positions 151 and 152 (PaNip7$^{R151A/R152A}$) and the other containing alanine residues at positions 155 and 158 (PaNip7$^{K155A/K158A}$). The mutant proteins were expressed in *E. coli* and purified for RNA binding assays. Binding of both mutant proteins to poly-U was drastically reduced as determined by EMSA (Figure 6), which strongly supports the hypothesis that residues R151, R152, K155, and K158 of PaNip7 are directly involved in RNA binding.

As described above and in Table 3, PaNip7 residues R151, R152, K155, and K158 are not conserved in the PUA domain of Nip7p and HsNip7 proteins, with equivalent positions being occupied by residues G160, I161, F164, and A167. We hypothesized that if involved in RNA interaction, residues I161 and F164 should play an important role since they contain larger side chains relative to glycine and alanine residues of positions 160 and 167, respectively. A mutant clone was constructed in which residues I161 and F164 were replaced by alanine. The recombinant mutant protein (Nip7p$^{I161A/F164A}$) was assayed for poly-U binding and, similarly to PaNip7 mutants, showed reduced RNA binding activity (Figure 6). This result is consistent with the direct involvement of residues I161 and F164 with RNA interaction.

DISCUSSION

The PUA domain has already been identified in approximately 600 proteins of different families (*38*), including a large number of uncharacterized proteins. In RNA-

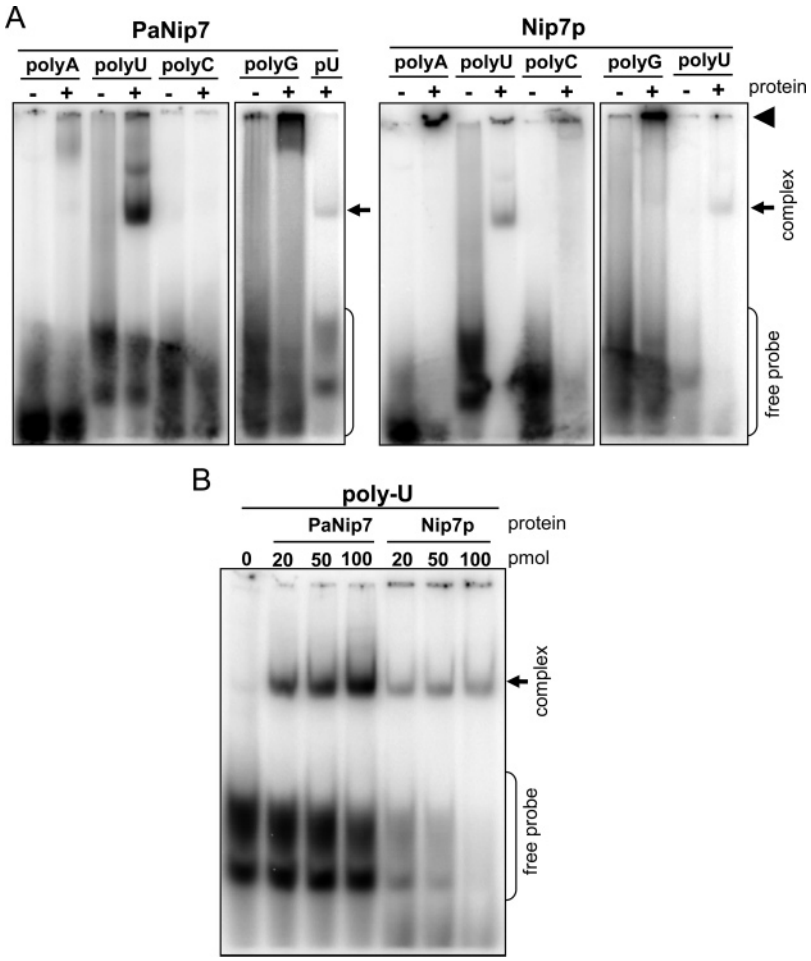

FIGURE 5: Analysis of yeast Nip7p and PaNip7 interaction with oligoribonucleotides. The panels show protein-RNA complexes resolved by electrophoretic mobility shift assays under native conditions on polyacrylamide gels and visualized by autoradiography as described in Experimental Procedures. (A) One picomole of the indicated oligoribonucleotides (poly-$A_{(25)}$, poly-$U_{(25)}$, poly-$C_{(25)}$ and poly-$G_{(18)}$) was incubated with 50 pmol of recombinant PaNip7 (left panel) or with recombinant yeast Nip7p (right panel). (B) One picomole of [^{32}P]-labeled poly-$U_{(25)}$ was incubated with increasing concentrations of recombinant PaNip7 or with recombinant yeast Nip7p. Arrows indicate the shifted bands corresponding to the complexes formed by PaNip7 and yeast Nip7p proteins with poly-U oligoribonucleotides. The arrowhead indicates the samples trapped in the wells.

modifying enzymes, the PUA domain function has been associated with RNA interaction. However, increasing evidence suggests that the PUA domain fold provides a structural scaffold for more general macromolecular interactions than initially thought (*38*). In *E. coli* glutamate 5-kinase, which displays a two-domain architecture with an N-terminal amino acid kinase (AAK) domain and a C-terminal PUA domain, the PUA domain has apparently assumed a role nonrelated to RNA processing, taking part in monomer interaction, in formation of a cavity at the dimer interface involved in magnesium binding, and binding a glutamate residue (*20*). The human candidate oncogene MCT1 shows a molecular weight similar to Nip7 proteins and contains a PUA domain in the C-terminal region. Unlike Nip7 PUA domains, this particular PUA domain was reported to interact with the mRNA cap translation factor complex, linking the MCT1 protein to translational control (*19*). In the *E. coli* methyltransferase YebU, which methylates cytidine$_{1407}$ of the 16S rRNA, the PUA domain forms a tight interface with the methyltransferase domain, and although there is no straightforward model that explains the mechanistic role played by the PUA domain of YebU (*17*), it still could be involved in RNA interaction during methylation of the 16S rRNA.

The experimental evidence for the mechanism of PUA domain interaction with RNA is based mostly on the crystal structures of the archaeal Cbf5 (*39*), TruB (*40*), and ArcTGT (*37*) proteins in complex with RNA that are currently available at PDB. In these complexes, the PUA domain contacts the RNA molecule using a glycine-containing loop which connects the first α-helix and the second β-strand and via residues from the sixth β-strand. RNA recognition depends on the identity of the $\alpha1-\beta2$ and $\beta6$ side chains involved in RNA interactions (reviewed in ref *38*). Corresponding regions in PaNip7 include helix α5 (PUA α1), the loop between α5 and the 3_{10} helix α6, and β-strand $\beta12$ (Figure 1). In Cbf5 and TruB, the PUA domains mediate the interaction with the minor groove of double-stranded RNA (*39*, *40*) whereas the ArcTGT PUA domain binds to the bottom of the $tRNA^{Val}$ acceptor stem, through the major groove (*37*). The structural alignment suggests that PaNip7 uses a mechanism similar to ArcTGT for RNA interaction, involving the positively charged residues R151, R152, K155, K158 from β-strand $\beta12$ (Figure 2). However, these residues are not structurally conserved in the yeast and human Nip7p counterparts, which are replaced by a glycine and three residues with hydrophobic side chain (Figure 3B, Table 3). In fact, the structure of the PUA domain from PaNip7

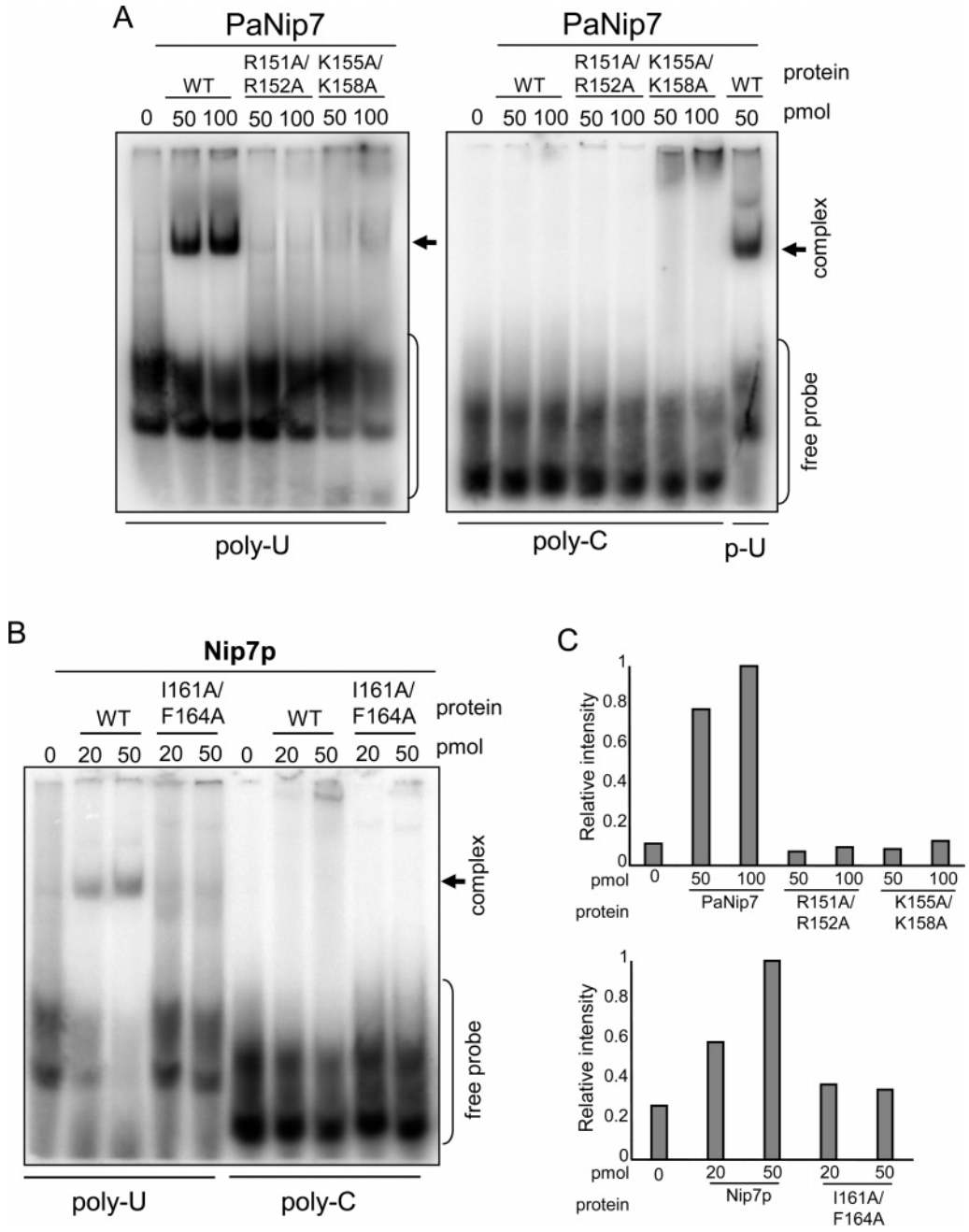

FIGURE 6: Analysis of the interaction of Nip7p and PaNip7 mutants with oligoribonucleotides. The panels show protein−RNA complexes resolved by electrophoretic mobility shift assays on polyacrylamide gels and visualized by autoradiography as described in Experimental Procedures. (A) One picomole of [^{32}P]-labeled poly-$U_{(25)}$ or poly-$C_{(25)}$ was incubated with 50 and 100 pmol of the recombinant wild type PaNip7 (WT) and of the mutant PaNip7$^{R151A/R152A}$ and PaNip7$^{K155A/K158A}$. p-U indicates the positive control in the assay containing [^{32}P]-labeled poly-$U_{(25)}$ and wild type PaNip7. (B) One picomole of [^{32}P]-labeled poly-$U_{(25)}$ or poly-$C_{(25)}$ was incubated with 20 and 50 pmol of the recombinant yeast wild type Nip7p (WT) and of the mutant Nip7$^{I161A/F164A}$. Arrows indicate the shifted bands corresponding to the complexes formed by PaNip7 and yeast Nip7p with poly-U. (C) Graphs showing the quantitation of the PaNip7-poly-U (top) and Nip7p-poly-U (bottom) complexes of the assays shown in A and B, respectively. The graphs show the intensity of the complexes relative to the lanes containing 100 pmol of PaNip7 or 50 of Nip7p, respectively, which were set to one.

revealed two differences relative to eukaryotic Nip7p and other archaeal PUA domains, which possess an insertion between β-strands β11 and β12 as compared to PaNip7 (residues 149 to 156 which form helix α7). The second difference involves the composition and distribution of positively charged residues that renders the PaNip7 PUA domain with a highly positive electrostatic surface and the Nip7p PUA domain with a predominantly hydrophobic surface. In Nip7p and HsNip7, electrostatic interaction between positively charged residues and phosphates of the RNA backbone would only be possible through a different region of the PUA domain involving residues K100, K115, and R154. In accordance with the structural comparisons, mutational analyses (Figure 6) have shown that residues R151, R152, K155, and K158 of PaNip7 are involved in RNA interaction. Mutational analysis of the yeast Nip7p has also shown that residues I161 and F164 are required for RNA interaction, indicating that the same region of the PUA domain interacts with poly-U in archaeal and yeast Nip7p proteins but probably via different contacts.

The *S. cerevisiae* ribosome biogenesis Rrp5p protein has also been described to preferentially bind poly-U and U-rich sequences (*41*). Rrp5p contains twelve tandem repeats of the S1 RNA binding domain in the N-terminal region that is responsible for RNA binding *in vitro* with a higher affinity to poly-U (*41*). Genetic depletion of Rrp5p results in accumulation of pre-rRNA species with extended 5′ end, affecting biogenesis of both ribosomal subunits. Based on deletion analyses of the pre-rRNA, de Boer and co-workers (*41*) have proposed that Rrp5p may bind to a conserved single-stranded U-rich sequence upstream from the pre-rRNA cleavage site A2 in ITS1. Genetic depletion of Nip7p results in accumulation of unprocessed 27S pre-rRNA (*7*), indicating that it is required for processing of ITS2. As many 60S biogenesis factors, Nip7p is not found in 90S preribosomes (*3*), and, consistent with the genetic depletion data, it cosediments with the 60S subunit peak in sucrose density gradients (*7*) and has been found associated with pre-60S complexes (*5*, *6*). Although the *in vitro* interaction assays indicated a low Nip7p affinity for the ITS2 region (Figure 4) even though it contains several U-rich stretches, Nip7p interacts with the nucleolar proteins, Nop8p and Nop53p (*9*, *10*), both containing RNA interaction domains, that may bind the pre-rRNA and help stabilize Nip7p on ITS2 *in vivo*. However, one has to consider also that the Nip7p preference for binding to poly-U raises the question whether *in vivo* Nip7 proteins might bind to U-rich snoRNAs instead of pre-rRNA sequences. Nip7p does not possess intrinsic catalytic activity and might function as an adaptor since it has the ability to bind to RNA via the C-terminal PUA domain and interacts with proteins involved in pre-rRNA processing, such as Rrp43p, Nop8p, and Nop53p (*9*, *10*), possibly via its N-terminal domain. The temperature sensitive *nip7-1* allele results from mutation of a conserved glycine residue at position 71 which is replaced by an aspartic acid (*7*), affecting Nip7p stability and interaction with other proteins in the yeast two-hybrid system (data not shown).

In conclusion, we have shown that the PUA domain of Nip7 proteins mediates interaction with RNA. Although RNA-binding assays did not identify a 35S pre-rRNA sequence to which Nip7p could bind specifically, we found that Nip7 proteins bind specifically to poly-U RNAs *in vitro*. Structural and mutational analyses revealed that equivalent regions, including residues R151, R152, K155, and K158 in PaNip7 and residues I161 and F164 in yeast Nip7p PUA domains, are involved in RNA interaction.

ACKNOWLEDGMENT

The authors are grateful to Zildene G. Correa for technical assistance. P.P.C., D.C.G., and J.S.L. are recipients of FAPESP fellowships.

SUPPORTING INFORMATION AVAILABLE

One figure showing the $2F_o - F_c$ electron density map calculated from experimental phases (contour level 1.2σ) of the PaNip7 refined model superposed to the experimental map, showing a region of the β9, β8, and β10 strands of the PUA domain (from left to right). This material is available free of charge via the Internet at http://pubs.acs.org

REFERENCES

1. Fromont-Racine, M., Senger, B., Saveanu, C., and Fasiolo, F. (2003) Ribosome assembly in eukaryotes, *Gene 313*, 17−42.
2. Peng, W. T., Robinson, M. D., Mnaimneh, S., Krogan, N. J., Cagney, G., Morris, Q., et al. (2003) A panoramic view of yeast noncoding RNA processing, *Cell 113*, 919−933.
3. Grandi, P., Rybin, V., Bassler, J., Petfalski, E., Strauss, D., Marzioch, M., et al. (2002) 90S pre-ribosomes include the 35S pre-rRNA, the U3 snoRNP, and 40S subunit processing factors but predominantly lack 60S synthesis factors, *Mol. Cell 10*, 105−115.
4. Dragon, F., Gallagher, J. E., Compagnone-Post, P. A., Mitchell, B. M., Porwancher, K. A., Wehner, K. A., et al. (2002) A large nucleolar U3 ribonucleoprotein required for 18S ribosomal RNA biogenesis, *Nature 417*, 967−970.
5. Bassler, J., Grandi, P., Gadal, O., Lessmann, T., Petfalski, E., Tollervey, D., Lechner, J., and Hurt, E. (2001) Identification of a 60S preribosomal particle that is closely linked to nuclear export, *Mol. Cell 8*, 517−529.
6. Nissan, T. A., Bassler, J., Petfalski, E., Tollervey, D., and Hurt, E. (2002) 60S pre-ribosome formation viewed from assembly in the nucleolus until export to the cytoplasm, *EMBO J. 21*, 5539−5547.
7. Zanchin, N. I. T., Roberts, P., DeSilva, A., Sherman, F., and Goldfarb, D. S. (1997) *Saccharomyces cerevisiae* Nip7p is required for efficient 60S ribosome subunit biogenesis, *Mol. Cell. Biol. 17*, 5001−5015.
8. Zanchin, N. I. T., and Goldfarb, D. S. (1999a) The exosome subunit Rrp43p is required for the efficient maturation of 5.8S, 18S and 25S rRNA, *Nucl. Acids Res. 27*, 1283−1288.
9. Zanchin, N. I. T., and Goldfarb, D. S. (1999b) Nip7p interacts with Nop8p, an essential nucleolar protein required for 60S ribosome biogenesis, and the exosome subunit Rrp43p, *Mol. Cell. Biol. 19*, 1518−1525.
10. Granato, D. C., Gonzales, F. A., Luz, J. S., Cassiola, F., Machado-Santelli, G. M., and Oliveira, C. C. (2005) Nop53p, an essential nucleolar protein that interacts with Nop17p and Nip7p, is required for pre-rRNA processing in *Saccharomyces cerevisiae*, *FEBS J. 272*, 4450−4463.
11. van Hoof, A., Staples, R. R., Baker, R. E., and Parker, R. (2000) Function of the Ski4p (Csl4p) and Ski7p proteins in 3′-to-5′ degradation of mRNA, *Mol. Cell. Biol. 20*, 8230−8243.
12. Mitchell, P., Petfalski, E., Shevchenko, A., Mann, M., and Tollervey, D. (1997) The exosome: a conserved eukaryotic RNA processing complex containing multiple 3′→5′ exoribonucleases, *Cell 91*, 457−466.
13. Sekiguchi, T., Todaka, Y., Wang, Y., Hirose, E., Nakashima, N., and Nishimoto, T. (2004) A novel human nucleolar protein, Nop132, binds to the G proteins, RRAG A/C/D, *J. Biol. Chem. 279*, 8343−8350.
14. Hesling, C., Oliveira, C. C., Castilho, B. A., and Zanchin, N. I. T. (2007) The Shwachman-Bodian-Diamond syndrome associated protein interacts with HsNip7 and its down-regulation affects gene expression at the transcriptional and translational levels, *Exp. Cell Res.*, in press.
15. Aravind, L., and Koonin, E. (1999) Novel predicted RNA-binding Domains Associated with the Translation Machinery, *J. Mol. Biol. 48*, 291−302.
16. Ishitani, R., Nureki, O., Fukai, S., Kijimoto, T., Nameki, N., Watanabe, M., et al. (2002) Crystal structure of archaeosine tRNA-guanine transglycosylase, *J. Mol. Biol. 318*, 665−677.
17. Hallberg, B. M., Ericsson, U. B., Johnson, K. A., Andersen, N. M., Douthwaite, S., Nordlund, P., Beuscher, A. E., IV, and Erlandsen, H. (2006) The structure of the RNA m^5C methyltransferase YebU from *Escherichia coli* reveals a C-terminal RNA-recruiting PUA domain, *J. Mol. Biol. 360*, 774−787.
18. Manival, X., Charron, C., Fourmann, J. B., Godard, F., Charpentier, B., and Branlant, C. (2006) Crystal structure determination and site-directed mutagenesis of the *Pyrococcus abyssi* aCBF5-aNOP10 complex reveal crucial roles of the C-terminal domains of both proteins in H/ACA sRNP activity, *Nucl. Acids Res. 34*, 826−839.
19. Reinert, L. S., Shi, B., Nandi, S., Mazan-Mamczarz, K., Vitolo, M., Bachman, K. E., He, H., and Gartenhaus, R. B. (2006) MCT-1 protein interacts with the cap complex and modulates messenger RNA translational profiles, *Cancer Res. 66*, 8994−9001.
20. Marco-Marín, C., Gil-Ortiz, F., Pérez-Arellano, I., Cervera, J., Fita, I., and Rubio, V. (2007) A novel two-domain architecture within

the amino acid kinase enzyme family revealed by the crystal structure of *Escherichia coli* glutamate 5-kinase, *J. Mol. Biol. 367*, 1431−1446.
21. Coltri, P. P., Guimarães, B. G., Oliveira, C. C., and Zanchin, N. I. T. (2004) Expression, crystallization and preliminary X-ray analysis of the *Pyrococcus abyssi* protein homologue of *Saccharomyces cerevisiae* Nip7p, *Acta Crystallogr.Sect. D: Biol. Crystallogr. 60*, 1925−1928.
22. Carneiro, F. R., Silva, T. C., Alves, A. C., Haline-Vaz, T., Gozzo, F. C., and Zanchin, N. I. T. (2006) Spectroscopic characterization of the tumor antigen NY-REN-21 and identification of heterodimer formation with SCAND1, *Biochem. Biophys. Res. Commun. 343*, 260−268.
23. Sambrook, J., Fritsch, E. J., and Maniatis, T. (1989) in *Molecular cloning, a laboratory manual*, 2nd ed., Cold Spring Harbor Laboratory Press, Cold Spring Harbor, NY.
24. Dauter, Z., Dauter, M., and Rajashankar, K. R. (2000) Novel approach to phasing proteins: derivatization by short cryo-soaking with halides, *Acta Crystallogr.Sect. D: Biol. Crystallogr. 56*, 232−237.
25. Nagem, R. A. P., Dauter, Z., and Polikarpov, I. (2001) Protein crystal structure solution by fast incorporation of negatively and positively charged anomalous scatterers, *Acta Crystallogr.Sect. D: Biol. Crystallogr. 57*, 996−1002.
26. Sheldrick, G. M., and Schneider, T. R. (2001) in *Methods in Macromolecular Crystallography* (Turk, D., and Johnson, L., Eds.) pp 72−81, IOS Press, Amsterdam.
27. La Fortelle, E., and Bricogne, G. (1997) Maximum-likelihood heavy-atom parameter refinement for multiple isomorphous replacement and multiwavelength anomalous diffraction methods, *Methods Enzymol. 276*, 472−494.
28. Abrahams, J. P., and Leslie, A. G. W. (1996) Methods used in the structure determination of bovine mitochondrial F1 ATPase, *Acta Crystallogr.Sect. D: Biol. Crystallogr. 52*, 30−42.
29. Perrakis, A., Morris, R., and Lamzin, V. S. (1999) Automated protein model building combined with iterative structure refinement, *Nat. Struct. Biol. 6*, 458−463.
30. Jones, T., Zou, J., Cowan, S., and Kjeldgaard, M. (1991) Improved methods for building protein models in electron density maps and the location of errors in these models, *Acta Crystallogr Sect. A: Found. Crystallogr. 47*, 110−119.
31. Murshudov, G. N., Vagin, A. A., and Dodson, E. J. (1997) Refinement of macromolecular structures by the maximum-likelihood method, *Acta Crystallogr.Sect. D: Biol. Crystallogr. 53*, 240−255.
32. Collaborative Computational Project, Number 4 (1994) The CCP4 suite: programs for protein crystallography, *Acta Crystallogr.Sect. D: Biol. Crystallogr. 50*, 760−763.
33. Laskowski, R. A., MacArthur, M. W., Moss, D. S., and Thornton., J. M. (1993) PROCHECK: a program to check the stereochemical quality of protein structures, *J. Appl. Crystallogr. 26*, 283−291.
34. Schwede, T., Kopp, J., Guex, N., and Peitsch, M. C. (2003) SWISS-MODEL: An automated protein homology-modeling server, *Nucl. Acids Res. 31*, 3381−3385.
35. Liu, J. F., Wang, X. Q., Wang, Z. X., Chen, J. R., Jiang, T., An, X. M., Chang, W. R., and Liang, D. C. (2004) Crystal structure of KD93, a novel protein expressed in human hematopoietic stem/progenitor cells, *J. Struct. Biol. 148*, 370−374.
36. Krissinel, E., and Henrick, K. (2004) Secondary-structure matching (SSM), a new tool for fast protein structure alignment in three dimensions, *Acta Crystallogr.Sect. D: Biol. Crystallogr. 60*, 2256−2268.
37. Ishitani, R., Nureki, O., Nameki, N., Okada, N., Nishimura, S., and Yokoyama, S. (2003) Alternative tertiary structure of tRNA for recognition by a posttranscriptional modification enzyme, *Cell 113*, 383−394.
38. Perez-Arellano, I., Gallego, J., and Cervera, J. (2007) The PUA domain - a structural and functional overview, *FEBS J.*, in press.
39. Li, L., and Ye, K. (2006) Crystal structure of an H/ACA box ribonucleoprotein particle, *Nature 443*, 302−307.
40. Pan. H., Agarwalla, S., Moustakas, D. T., Finer-Moore, J., and Stroud, R. M. (2003) Structure of tRNA pseudouridine synthase TruB and its RNA complex: RNA recognition through a combination of rigid docking and induced fit, *Proc. Natl. Acad. Sci. U.S.A. 100*, 12648−12653.
41. de Boer, P., Vos, H. R., Faber, A. W., Vos, J. C., and Raué, H. A. (2006) Rrp5p, a trans-acting factor in yeast ribosome biogenesis, is an RNA-binding protein with a pronounced preference for U-rich sequences, *RNA 12*, 263−271.

BI7015876

SUPORTING INFORMATION

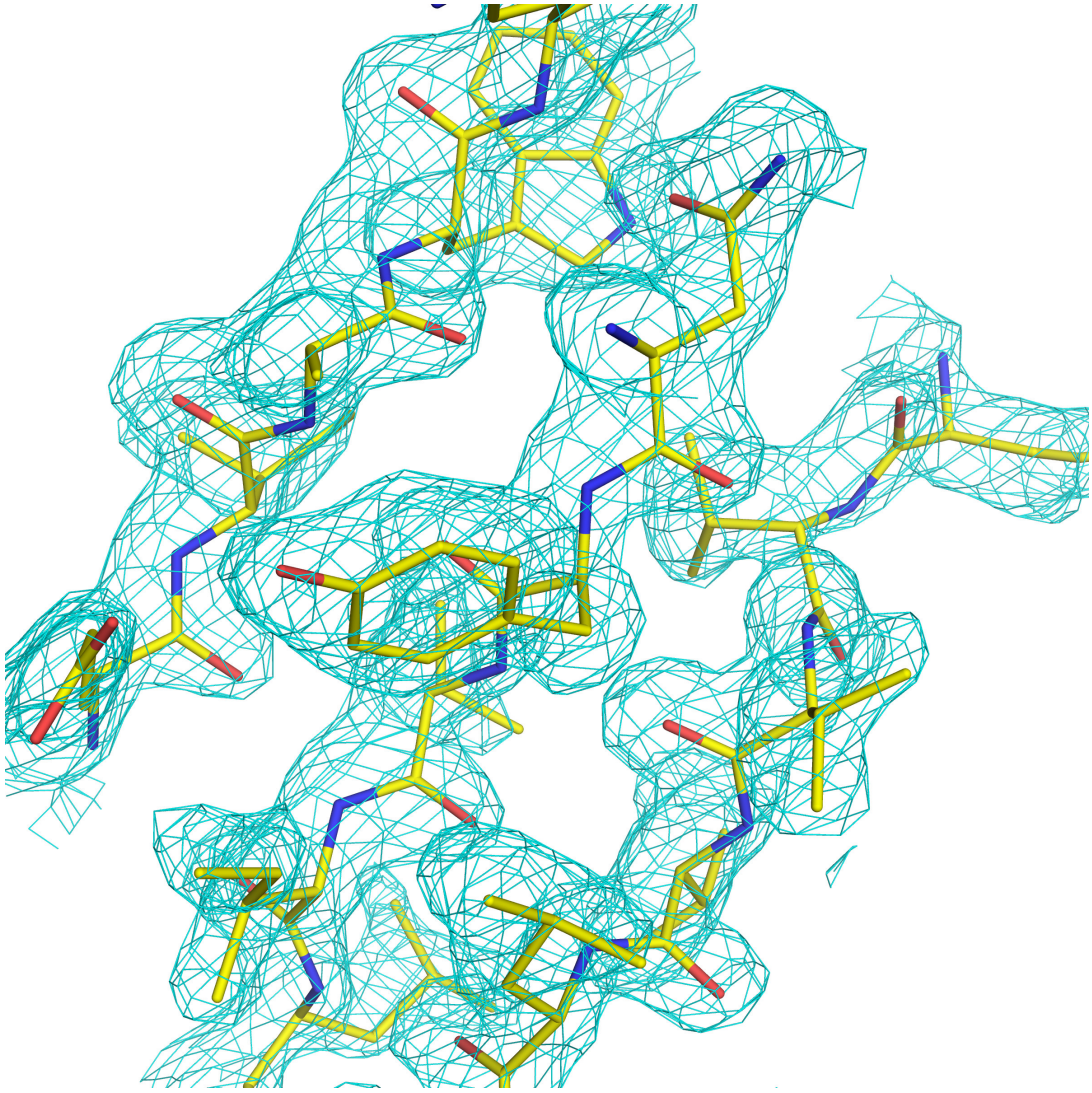

Figure S1. 2Fo-Fc electron density map calculated from experimental phases (contour level 1.2σ). The PaNip7 refined model is superposed to the experimental map, showing a region of the β9, β8 and β10 strands of the PUA (from left to right). Tyrosine 97 is shown in the center.